Published in final edited form as:
J Am Chem Soc. 2013 May 29; 135(21): 8078–8088. doi:10.1021/ja403842j.

Amino acid substitution in the active site of DNA polymerase β explains the energy barrier of the nucleotidyl transfer reaction

Vinod K. Batra[†], **Lalith Perera**[†], **Ping Lin**[¶], **David D. Shock**[†], **William A. Beard**[†], **Lars C. Pedersen**[†], **Lee G. Pedersen**[†,‡], and **Samuel H. Wilson**[†,*]

[†]Laboratory of Structural Biology, National Institute of Environmental Health Sciences, National Institutes of Health, P.O. Box 12233, Research Triangle Park, NC 27709-12233

[‡]Department of Chemistry, CB3290, University of North Carolina at Chapel Hill, Chapel Hill, NC 27599

[¶] Penn State University, 320 Steidle PSU, University Park, PA, 16802

Abstract

DNA polymerase β (pol β) is a bifunctional enzyme widely studied for its roles in base excision DNA repair where one key function is gap-filling DNA synthesis. In spite of significant progress in recent years, the atomic level mechanism of the DNA synthesis reaction has remained poorly understood. Based on crystal structures of pol β in complex with its substrates and theoretical considerations of amino acids and metals in the active site, we have proposed that a nearby carboxylate group of Asp256 enables the reaction by accepting a proton from the primer O3′ group, thus activating O3′ as the nucleophile in the reaction path. Here, we tested this proposal by altering the side chain of Asp256 to Glu and then exploring the impact of this conservative change on the reaction. The D256E enzyme is more than 1,000-fold less active than the wild-type enzyme, and the crystal structures are subtly different in the active sites of the D256E and wild-type enzymes. Theoretical analysis of DNA synthesis by the D256E enzyme shows that the O3′ proton still transfers to the nearby carboxylate of residue 256. However, the electrostatic stabilization and location of the O3′ proton transfer during the reaction path are dramatically altered compared with wild-type. Surprisingly, this is due to repositioning of the Arg254 side chain in the Glu256 enzyme active site, such that Arg254 is not in position to stabilize the proton transfer from O3′. The theoretical results with the wild-type enzyme indicate early charge reorganization associated with the O3′ proton transfer, and this does not occur in the D256E enzyme. The charge reorganization is mediated by the catalytic magnesium ion in the active site.

Introduction

DNA polymerases are fundamental to the replication and repair of the genomic material throughout the domains of life, from the most primitive organisms to vertebrates. In most cases organisms maintain more than one DNA polymerase isoform, and these enzymes often function in combination with accessory factors and other enzymes to perform specialized tasks in DNA metabolism.[1-4] There are many examples where a DNA polymerase polypeptide chain itself carries an additional accessory-type enzymatic activity.[1] The DNA polymerase, or nucleotidyl transferase, function of these enzymes is generally thought to require two metal ions as co-factors, along with dNTPs and a DNA 3′-end as the substrates.[5,6] The enzymes use DNA as a cofactor for both template-directed selection of

*Corresponding Author: Laboratory of Structural Biology, National Institute of Environmental Health Sciences, National Institutes of Health, P.O. Box 12233, Research Triangle Park, NC 27709-12233, wilson5@niehs.nih.gov.

dNTP substrates and as the substrate for nucleotide insertion into the 3′-end of a nascent DNA strand. The reaction products are the dNMP extended DNA strand and the resulting pyrophosphate. DNA polymerases are often capable of performing the reverse reaction, producing dNTPs using as substrates pryophosphate and the 3′-terminal nucleotide of a DNA strand.[7] Through studies of these enzymes isolated from many different organisms in the phylogenetic tree, it seems clear that they use a generally conserved mechanism for nucleotidyl transfer. On the other hand, the mechanisms governing the actual efficiency of the DNA polymerase nucleotidyl transferase reaction are still not well understood. This topic is important because DNA polymerases exhibit a wide range of enzymatic efficiencies for DNA synthesis, and this feature is key in the fidelity for template-directed nucleotide incorporation: the higher the efficiency for correct nucleotide insertion, the higher the fidelity.[8] Thus, differences in enzymatic efficiency and fidelity appear to reflect important specialized functions of these enzymes in DNA replication and repair. In the case of mammalian DNA polymerase β (pol β), the DNA synthesis function appears to be gap filling of short gaps formed during DNA repair and replication, and the speed and accuracy of such gap filling synthesis is fundamental to maintaining genomic stability. In light of its small size (~39 kDa), its activity as a monomer, and the fact that it is well behaved in kinetic and structural studies, pol β is viewed as a model enzyme for understanding DNA synthesis mechanisms.

The molecular features responsible for modulating the differences in enzymatic efficiency for alternate DNA polymerases are still obscure. Yet, at the heart of the issue is understanding electrostatic features that are linked to chemistry; i.e., features that hasten formation of the transition state (TS) and stabilize the products. DNA polymerases use a “two-metal-ion mechanism” to increase the rate of template base-directed DNA synthesis by many orders of magnitude over the uncatalyzed reaction in aqueous solution.[5] These enzymes promote nucleophilic attack by the primer O3′ atom on the α-phosphate (Pα) of the deoxnucleoside 5′-triphosphate selected for template-directed insertion into the primer strand. Previous research had shown that nucleotide insertion results in stereo-inversion of the non-bridging oxygens about Pα.[9] Various computational analyses making use of crystal structures of ternary substrate complexes of DNA polymerases poised for chemistry have suggested different options for activation of O3′ nucleophilic attack on Pα. For example, a combined quantum mechanics and molecular mechanics computational analysis of the pol β reaction (refs as noted) revealed transfer of the O3′ proton in the ground state to a nearby aspartate (Asp256) early in the reaction coordinate and then $O3'^{-}$ attack at Pα. In contrast, Cisneros et al. using the λ polymerase and a different computational approach found that O3′ proton transfers late in the reaction coordinate, just prior to O3′ attack on Pα.[10]

The mechanism of proton transfer from O3′ and the spatial and temporal properties of the transfer are important features in understanding the polymerase reaction mechanism. This is because of both steric and charge considerations must be accommodated during the nucleotidyl transfer reaction, as the oxyanion ($O3'^{-}$) approaches Pα during transition state (TS) development. The metal ions and enzyme side chains in the vicinity of this bond-forming step must stabilize the charges and steric features in the system, but insight on possible mechanisms of how this is accomplished is still lacking. For one aspect of the mechanism, Liu et al. observed O3′ proton transfer to a nearby water molecule with eventual proton transfer to an oxygen on the γ-phosphate, and Nakamura et al. recently proposed O3′ proton transfer to a nearby water molecule from observing phosphodiester bond formation in crystals of DNA polymerase η.[11,12]

For pol β, computational and crystallographic studies indicated that the O3′ proton transfers to the OD2 oxygen of the nearby aspartate side chain (Asp256).[13] In the “ground state” before the reaction proceeds (Scheme 1), there is a hydrogen bond between O3′ and the OD2

oxygen of Asp256. The OD2 oxygen of this aspartate also coordinates the catalytic metal (Mg^{2+}_{cat}).

The guanidine-group of an adjacent arginine side chain (Arg254) stabilizes the carboxylate of Asp256 through interaction with OD1. This network of interactions in the ground state pre-chemistry complex integrates well with the results of computational analyses in that the proximity of O3′ to OD2 of Asp256 enabled proton transfer with a minimal energy cost and early in the energy landscape of the reaction path.[13]

In the present study, we further examined the role of the Asp256 side chain in the O3′ proton transfer step of the pol β reaction mechanism by substituting glutamate for the aspartate at residue 256 (i.e., the D256E mutant). The aim was to make a subtle change in the atomic position of the carboxylate side chain, and then investigate the affect of the alteration on the structure, reaction kinetics and computationally derived energy landscape for the DNA synthesis reaction. The D256E enzyme insertion rate is decreased over 3-orders of magnitude relative to wild-type enzyme, and the crystal structure revealed that the carboxylate group of the D256E side chain is in a different location than that of the wild-type aspartate side chain. Yet, like OD2 of Asp256, OE1 of the D256E enzyme is in position to accept the O3′ proton. Surprisingly, a striking difference between the wild-type and D256E enzymes was observed for the Arg254 side chain. The salt-bridge interaction in the wild-type enzyme between Arg254 and Asp256 is not present in the mutant; instead, Arg254 is displaced from the vicinity of the 256 side chain. In the computational assessment, the energy landscape of the reaction path for D256E was different from that of the wild-type enzyme, including the observation that the O3′ proton transfer failed to occur until late in the reaction path. The results are discussed in terms of differences in charge distributions and electrostatic stabilizations for the mutant and wild-type systems for O3′ attack on Pα, including new roles for the active site metal ions.

Experimental Design

Crystallization of the Pol β Mutants Substrate Complex

Human pol β mutants (D256E and D256A) were over-expressed in *E. coli* and purified as described earlier.[14] Binary complex crystals with these mutants with a 1-nucleotide gapped DNA were grown as previously described.[15] The sequence of the template strand (16-mer) was 5′- CCG ACA GCG CAT CAG C- 3′. The primer strand (10-mer) sequence was 5′- GCT GAT GCG C -3′. The downstream oligonucleotide (5-mer) was phosphorylated, and the sequence was 5′- GTC CC -3′. The binary complex crystals were then soaked in artificial mother liquor (50 mM imidazole, pH 7.5, 20% PEG3350, 90 mM sodium acetate, 200 mM $MgCl_2$ with 5 mM non-hydrolyzable dNTP analog, dUMPNPP) and 12% ethylene glycol as cryoprotectant. This resulted in ternary complex crystals. Diffraction quality data was collected on those ternary complex crystals as described.

Data collection and structure determination

Data were collected at 100°K on a CCD detector system mounted on a MiraMax®-007HF (Rigaku Corporation) rotating anode generator. Data were integrated and reduced with HKL2000 software.[16] The mutant crystal structures have similar lattices to the previously determined ternary complex (PDB Code: 2FMS) and are sufficiently isomorphous to allow direct refinement, followed by multiple rounds of model building in O and refinement in CNS or PHENIX.[15] The figures were prepared in Chimera.[17]

Kinetic measurements

To directly measure the rate of the first insertion (k_{pol}), single-turnover kinetic assays (enzyme/DNA = 5 or 10) were performed as outlined previously.[18] Slow reactions were started/quenched manually and faster reactions were measured with a KinTek Model RQF-3 chemical quench-flow apparatus (KinTek Corp., Snow Shoe, PA). Briefly, a solution of pol β (0.5–1 μM) was preincubated with single-nucleotide gapped DNA (100 nM) with a templating guanine in the gap. This solution was rapidly mixed (2-fold dilution) with 200 μM dCTP and 20 mM $MgCl_2$. The final reaction conditions also included 50 mM Tris-HCl, pH 7.4 (37 °C), and 100 mM KCl. After various time periods, the reactions were stopped with 0.3 M EDTA and the quenched samples were mixed with an equal volume of formamide dye, and the products separated on 15–16% denaturing polyacrylamide gels. The dried gels were analyzed using a PhosphorImager (Molecular Dynamics) to quantify product formation.

To measure the pH-dependence of k_{pol}, a buffer mixture was used consisting of 50 mM MES, 25 mM Tris, 25 mM ethanolamine, 100 mM KCl.[19] The pH was adjusted with either HCl or NaOH as appropriate. The ionic strength of this buffer system is constant at the pH values used in this study.[20] The buffer was supplemented with 10% glycerol, 1 mM dithiothreitol, and 100 μg/mL bovine serum albumin. Products were separated as described above. Since a 6-carboxyfluorescein 5′-labeled primer was used in these assays, the products were quantified using the phosphorimager in fluorescence mode (532 nm laser with 526 nm shortpass filter). The pH dependence of k_{pol} was fit to function describing a single ionization: $k_{pol} = k_{ind}/(1 + 10^{pKa\text{-}pH})$ where k_{ind} is the pH-independent rate constant.

QM/MM computational analyses

Using X-ray crystal structures of the gapped DNA, dNTP analog, and pol β (wild-type and D256E mutant) ternary complexes as the starting points, molecular dynamics simulations were carried out in a completely solvated aqueous environment. Valence-filling hydrogens were added and the systems were neutralized with counter ions while preserving the positions of all the crystal water molecules. The initial triphosphate charge was set to −3 with only one oxygen protonated in the gamma-phosphate for the equilibration with the classical force field. The Amber99SB force field was used with the pmemd module of the Amber11 program for the trajectory calculations.[21,22] Water molecules were represented by the TIP3P model.[23] Long-range interactions were treated with the particle mesh Ewald method[24,25]. The added water molecules were subjected to a constant pressure simulation at low temperatures (<10°K) so that the starting system was at a density near 1g/cc. Except for the added waters and the counter-ions, all heavy atoms in the system were constrained to the crystal positions using a harmonic restraining force with a decreasing force constant from 50 kcal/mol/nm to 0.5 kcal/mol/nm during 10 ns simulations at 300°K at constant volume. This procedure ensures that the X-ray crystallographic coordinates that represent a configuration resembling the pre-catalytic state is not undergoing dramatic perturbation by the molecular dynamics simulation. The final configuration was energy minimized before initiating the QM/MM steps.

The QM/MM systems were prepared in the following way. The quantum region includes parts of Asp190, Asp192, Asp256 (or Glu256 in the mutant case), the primer terminal nucleotide, and dTTP, two Mg ions, and two water molecules coordinating the Mg ions (one on each in the wt case) and three waters in the D256E mutant case (two on Mg_{cat}). Atoms within 10 Å of the quantum atoms were treated using a classical MM force field and allowed to move. The remainder of the protein, DNA and counter ions were held stationary. Solvent water molecules within 15 Å, but farther than 10 Å of the QM atoms, were included and held fixed during the calculation. There were 9562 and 9692 atoms included in the QM/MM

calculations of the wild-type enzyme and D256E mutant, respectively. The charge for the QM region was −2 and the MM region was +2 while the total system remained neutral.

The hybrid QM/MM potential in the ONIOM (MO: MM) method implemented in the program, Gaussian09-B01 was used to investigate the bond formation during the reaction scheme.[26,27] The quantum region was treated using the B3LYP exchange correlation function and 6-31g* basis set.[28] The classical region was handled using the Amber ff99 force field within Gaussian09. Calculations were performed with the electronic embedding option to accommodate the polarization of the QM region by the partial atomic charges in the MM region and to provide for the response of the QM region, for which Merz-Kollman (MK) charge fitting was employed to generate partial charges at quantum atoms for classical interactions.[29]

In the previous QM/MM calculations on similar systems, various combinations of bond restrictions have been used to define the reaction path and energy coordinate. In the present study, on the other hand, we restricted analysis of the reaction to reductions in the O3′-Pα distance alone. This procedure not only reduced uncertainty in the interaction energy arising from additional constraints, but also allowed for the possibility of proton transfer to any other atom in the selected QM system. In this way, multiple alternate reaction paths were not excluded, as is the case in some schemes for defining a reaction coordinate. Here, we evaluated the wild-type and mutant systems with various possibilities for the location of the "O3′ proton" in the starting or un-reacted system: a) with the proton on O3′; and b) with the proton on OD2 of D256 (or OE1 of Glu256 in the mutant case). For comparison, we also examined additional proton locations (see Supplement): a) in the mutant case, with the proton on the water molecule that occupies the position of OD2 in wild-type; and b) with the proton on the dNTP oxygen, O5′, linking the sugar to the triphosphate. The transfer of O3′ proton to the water molecule or the O5′ oxygen occurred at very high energy (>40kcal/mol), suggesting these are not viable pathways.

Results

Previously we had used QM/MM computational analyses and the ternary complex crystal structure of wild-type pol β to assess the reaction path for the nucleotidyl transfer reaction with a correct incoming deoxynucleotide.[13] An important feature emerging from this work was transfer of the O3′ proton onto the adjacent oxygen (OD2) of Asp256 (Scheme 1); this occurred early in the reaction path and with a minimal energy barrier. In the present study, we explored the importance for this nearby OD2 oxygen of Asp256 in the O3′ proton transfer step of DNA synthesis. We prepared two pol β mutants with side chain alterations at residue 256, i.e., D256E and D256A, and determined their crystal structures and kinetic properties for DNA synthesis. Based on the results, a computational assessment of the nucleotidyl transferase reaction path for the D256E enzyme was then conducted, and the results were compared with those obtained with the wild-type enzyme, re-assessed here under the same conditions.

I) Crystal structures of the mutant enzymes

The structures of the D256E and D256A enzymes in ternary complex with gapped DNA and a correct incoming nucleotide were obtained at 2.0 and 2.4 Å resolution, respectively (Table 1).

The structures reveal the enzymes are in the closed conformation, and both structures are very similar to that of the ternary complex of the wild-type enzyme, i.e., 326 Cα rmsd of 0.17 and 0.22 Å for D256E and D256A, respectively (Fig. 1).

There are important differences, however, between the wild-type and mutant enzymes in the vicinity of the active sites. As expected, the residue 256 side chains are different: for the D256E enzyme (Fig.2A), the glutamate side chain is shifted away from Mg_{ca}compared with aspartate of the wild-type enzyme (Fig. 2B), and the carboxylate oxygens are not in position to coordinate the catalytic metal; however, O3′ is hydrogen bonded to a carboxylic oxygen (OE1) of Glu256. In the structure of the D256E enzyme, a water molecule occupies the same position as OD2 of Asp256 in the wild-type enzyme structure. This water molecule is hydrogen-bonded to O3′ (primer terminus), OE1 of Glu256, and coordinates the catalytic metal (Fig. 2A). In the D256E enzyme (Fig. 2A), O3′ is in position for in-line attack on Pα, and the distance between O3′ and Pα is 3.5 Å, a distance similar to the corresponding distance (3.4 Å) observed with wild-type enzyme, the structure of which is shown for comparison in Figure 2B. In contrast to the D256E mutant, alanine substitution has a large distortion in the active site (Fig. 3): O3′ is out of position for in-line attack on Pα (distance between O3′ and Pα is 4.9 Å) and the catalytic metal is not observed. On the other hand, the structures of the wild-type, D256E, and D256A enzymes are similar regarding the nucleotide metal (Mg_{nuc}), its ligands (Asp190 and Asp192), water molecules, and non-bridging oxygens of the incoming nucleotide triphosphate group (Figs. 2 and 3). In each case, the conformation of the incoming nucleotide and its triphosphate moiety is similar, including the presence of a hydrogen bond between O3′ of the incoming nucleotide and a non-bridging oxygen on its Pβ. The salt-bridge interaction between Asp256 and Arg254 seen in wild-type enzyme is not present in the D256E structure, and the Arg254 side chain is in a completely different position (Fig. 4). As will be described below, this difference in location of the Arg254 side chain appears to be an important feature responsible for differences between the D256E and wild-type enzymes.

II) Kinetic assessment of the D265E and D256A pol β mutants

The D256E enzyme retained enzymatic activity for gap-filling DNA synthesis, but its insertion rate (k_{pol}) was lower than that of the wild-type enzyme by more than 3 orders of magnitude: the D256A mutant, on the other hand, lacked significant enzymatic activity at pH 7.4 (Fig. 5A).

The insertion rate of wild-type pol β increases with increasing pH and fit to a model with one-ionizable group with a pK_a of 8.1 ± 0.05 (Fig. 5B).[31] This pK_a is similar to that measured for rat pol β and believed to reflect deprotonation of the primer terminus O3′.[32,33] Although D256A has negligible activity at neutral pH, it regains detectable activity at higher pH. Figure 5B shows that k_{pol} increases 10-fold per pH unit up to pH 10, the highest pH accessible for kinetic studies, and the pK_a is estimated to be ~11.7 ± 2.3. However, since there is little evidence of what the maximal achievable independent rate may be for this mutant, this pK_a should be considered a minumum value. Like the D256A mutant, k_{pol} of D256E also increases with increasing pH. In this case, the data fit a model where the pK_a = 9.5 ± 0.07 and k_{ind} = 0.45 ± 0.03 1/s.

III) Computational analysis of the nucleotidyl transfer reaction by wild-type pol β and D256E

We employed a QM/MM approach to determine reaction paths, intermediates, transition states, and atomic charges for the metal ions and other active site atoms in the wild-type and D256E systems. We had previously conducted QM/MM analyses of correct and incorrect insertions by the wild-type pol β, and those studies involved mapping reaction path energies as a function of both bond forming and bond breaking distances.[13,34] In contrast, for the present study, we used an alternate approach of reducing mapping variables to that of bond forming distance only. This approach involved fewer constraints than before and enhanced reaction path analysis; we applied a direct comparison of the wild-type and D256E systems.

For the comparison, the same basis set was used at all levels for atoms in the quantum calculation.

Wild-type enzyme reaction path—In the ground state (Fig. 6A), both OD2 of Asp256 and O3′ are coordinated with Mg_{cat}, and O3′ is hydrogen-bonded to OD2 at a distance of 2.8 Å. As the reaction path proceeds, the O3′ proton is transferred to OD2 of Asp256 (Fig. 6B). This proton transfer occurs early in the reaction path, at the O3′ to Pα distance of ~ 3.2 Å (Fig. 6).

The reaction path proceeds to the transition state (TS), corresponding to the O3′ to Pα bond forming distance of ~2.2 Å and bond breaking distance of 1.9 Å. The value of the energy barrier is ~14 kcal/mol (Fig. 6). We also note that a quantum mechanical cluster calculation (see Supplement) gave a similar energy barrier (~12 kcal/mol), but this was only when the protonation state of the dNTP was as described for the QM/MM calculation.

D256E enzyme reaction path—In the structure of the D256E system (Fig. 2A), the glutamate side chain's OE1 oxygen is not coordinated to Mg_{cat}, but OE1 is hydrogen bonded to O3′. However, the reaction path (Fig. 7) was found to be strikingly different from that of the wild-type system. First, as the reaction path proceeds from the ground state (Fig. 7), the energy is much lower with the proton remaining on O3′ than on OE1. As the reaction path proceeds with the O3′ proton remaining in place, energy builds until the O3′ proton transfers to OE1. The transition state is at the O3′ to Pα distance of ~2.2 Å, and the value of the energy barrier is ~21 kcal/mol. During the reaction path as O3′ approaches Pα, the proton transfer occurs at the O3′ to Pα distance of ~2.4 Å, very close to the transition state (Fig. 7). We also considered an alternate model where the O3′ proton is on OE1 throughout the entire reaction path. There was a substantial energy penalty of 8 to 10 kcal/mol in this case, ruling out this possibility.

Energy decomposition and non-quantum residue contribution—Electrostatic effects on the energy barrier for 10 amino acid residues located in the non-quantum region were estimated. The positions of these residues in the structure are illustrated in Fig. S1, and the effects for the residues are summarized in Table 2; the corresponding effects with the wild-type enzyme are also shown for comparison.

Energy values (kcal/mol) were computed by eqn. 1 in the Supplement. A minus value is stabilizing, and a plus value is destabilizing. Only those residues in non-quantum region with a significant effect are shown. Four of these residues, Arg183, Ser180, Arg149 and Arg40, have stabilizing effects in the D256E system, effects also mirrored in the wild-type system. Destabilizing effects in both systems were observed for Arg258, Lys234, Asp276 and Glu335.

A large difference between the wild-type and D256E systems was found for residue Arg254. This side chain is stabilizing for the D256E system (−6.0 kcal/mol), but destabilizing for the wild-type system (33.6 kcal/mol). As noted above, Arg254 has a salt-bridge interaction with the OD1 oxygen of Asp256 in the wild-type system, but is not in position to interact with the D256E carboxylate in the mutant system (Fig. 4). Finally, Glu295 is stabilizing for the D256E system and slightly destabilizing for wild type.

Charge analysis for Mg_{cat}, Mg_{nuc} and O3′—QM analysis of the charge associated with the two metal ions and O3′ throughout the reaction path revealed important differences between the wild-type and D256E systems (Fig. 8).

During the reaction path in the D256E system, Mg_{cat} and Mg_{nuc} exhibited gradual, steady increases in charge (loss of electron density) (Fig. 8A). Upon transfer of the O3′ proton to OE1, there were only modest changes throughout the remainder of the reaction path. In sharp contrast, in the wild-type system (Fig. 8B) charges of Mg_{cat} and Mg_{nuc} in the ground state were higher compared with those in D256E (e.g., Mg_{cat} +1.64e for wild-type vs. +1.08e for D256E). In addition, Mg_{cat} exhibited a large decrease in charge (increase in electron density) at a point near the beginning of the reaction path (i.e., decrease from +1.64e to +1.21e) (Fig. 8B). This corresponded to O3′ proton transfer to Asp256 OD2. After this point, Mg_{cat} exhibited a gradual increase in charge (loss of electron density), as the reaction path proceeded, whereas the Mg_{nuc} charge remained constant. Upon reaching the TS, Mg_{cat} now had a restored charge of +1.54e. Since the residue 256 carboxylate in the D256E system is not coordinated to Mg_{cat}, it was not surprising that Mg_{cat} in this case did not participate in a similar charge transfer (Fig. 8A).

Charge analysis for O3′ in the wild-type system revealed that the O3′ charge increased modestly with the proton transfer and then decreased somewhat (Fig. 8B). In the D256E system, the O3′ charge increased in a steady fashion until the proton transfer to OE1 (Fig. 8A), and then decreased until the TS. The O3′ charge for D256E system never reached the maximum value found for the wild-type system. In summary, for the wild-type enzyme, it appears that coordination between Asp256 OD2 and Mg_{cat} influences O3′ proton transfer by modulating the O3′ charge: the shift of charge to Mg_{cat} may facilitate association between O3′ and Pα. Similar charge analysis for other atoms in the vicinity of the catalytic metal also was conducted (Fig. S2). In the wild-type enzyme, the D256 OD2 charge decreased with the proton transfer (Fig. S2B), and a similar decrease in charge was observed with D256E OE1 (Fig. S2A).

Electrostatic attraction between O3′and Pα—Charge differences along the reaction path for O3′ and Pα can be evaluated to estimate their electrostatic attraction. In the beginning of the reaction path, the wild-type system O3′ to Pα electrostatic interaction is more attractive (~100 kcal/mol) compared to that in the D256E system (~43 kcal/mol). Throughout the reaction paths this difference is maintained until the transition states were reached; at this point for wild-type, the attraction is ~175 kcal/mol and for D256E, the attraction is ~100 kcal/mol. Thus, from the beginning of the reaction path to the transition states, the wild-type system was favored.

We conducted a further test of this interpretation by computing energy barriers for the wild-type and D256E systems after eliminating the electronic embedding of the ONIOM procedure; this minimizes electrostatic effects of the non-quantum residues and focuses on the active site quantum region. The TS barrier for the wild-type system increases from 14 to 42 kcal/mol, whereas for the D256E system it increases from 21 to 58 kcal/mol. That is, the electronic embedding procedure accounts for a >16 kcal larger increase in the D256E system than in the wild-type system, whereas the full calculation shows a difference between the two systems of ~7 kcal/mol. Another important point is that the Arg254 destabilizing effect observed in the wild-type system (Table 2) can be rationalized. The proton transfer from O3′ to Asp256 brings the proton closer to the positively charged guanidino group of Arg254, and the attendant repulsive effect is seen in the energy decomposition (Table 2). But once the repulsion is overcome early in the reaction path, the reaction now experiences a lower TS barrier, as the appropriately charged O3′ and Pα interact.

Discussion

The DNA polymerase active site includes three conserved acidic residues that bind two divalent magnesium ions. One magnesium ion (Mg_{nuc}) is coordinated by two aspartate

residues (Asp190 and 192 of pol β) and the triphosphate moiety of the incoming nucleotide thereby facilitating nucleotide binding. The other magnesium ion (Mg_{cat}) coordinates all three acidic residues and O3′ of the primer terminus. It's role is to lower the pK_a of the primer terminus O3′ and therefore is essential for catalytic activity. The third acidic residue is either a glutatmate or aspartate (pol β Asp 256), and since it coordinates the catalytic metal and O3′ is expected to also modulate the pK_a of the primer terminus.

The structures of the mutant enzymes and the pH profiles of activity are consistent with these proposals. With wild-type enzyme, the structure of the pre-catalytic ground state complex indicates that Asp256 coordinates both the catalytic magnesium ion and O3′.[15] The pH profile of activity indicates that nucleotide insertion increases with pH involving one deprotonation (pK_a = 8.1).[31] Although the rate of nucleotide insertion is severely diminished with alanine or glutamate substitution at residue 256, significant activity can be recovered by raising the pH of the assay (Fig. 5B). For the D256E mutant, the pH profile indicates that the pK_a of O3′ is not reduced to the same extent as wild-type enzyme (observed pK_a~9.5). The mutant enzyme structure reveals that this glutamate side chain coordinates O3′, but not the catalytic metal. A water molecule replaces the acidic side chain OD2 in the first coordination sphere of Mg_{cat} (Fig. 2A). The structure of the alanine mutant (D256A) confirms that O3′ is no longer coordinated to an acidic residue and the pK_a of the pH profile (Fig. 5B, ~11.6) is similar to that expected of deoxyribose (pK_a ~12.6).[35]

We assessed the activation of the primer O3′ nucleophile in the nucleotidyl transferase reaction by DNA polymerase β. The analysis was by QM/MM computational studies and was based on crystal structures of the wild-type and the D256E enzymes. The structures of the ternary enzyme/DNA/dNTP complexes showed the enzymes in the closed conformation, and the pre-catalytic structures provided a starting point for comparison of the reaction paths of the mutant and wild-type enzymes. The structures revealed different positions for the aspartate and glutamate carboxylate groups, but both were able to form a hydrogen bond with O3′ and accept the O3′ proton. The D256E enzyme was found to be 1000-fold less active than wild-type (Fig. 5A). The computational analyses revealed a striking difference in the temporal sequence of events in D256E compared with wild-type. With D256E, the O3′ proton remained in place until the O3′ to Pα bond forming distance was near that of the TS (Fig. 7). At this point, the proton moved to OE1 of D256E (Fig. 7C). For D256E, the energy barrier was ~21 kcal/mol. In contrast, for the wild-type enzyme the energy barrier was ~14 kcal/mol (Fig. 6) with the proton transfer from O3′ to OD2 early in the reaction path (Fig. 6B).

Analyses of these results help explain the mechanism of activation of the O3′ nucleophile in the nucleotidyl transfer reaction of wild-type pol β. The early transfer of the O3′ proton to OD2 of Asp256 may be expected to result in an increase in negative charge on O3′. Interestingly, however, there was synchronous transfer of charge from O3′ into Mg_{cat}, i.e., coupled with movement of the proton from O3′ to Asp256. Thus, a drop in charge of Mg_{cat} was found at the point in the reaction path corresponding to the proton transfer (Fig. 8B) and this was consistent with the relatively low pK_a of O3′ (Fig. 5B). In contrast, the charge of O3′ increased modestly at this point and then remained constant throughout the reaction path until just before the TS (Fig. 8B). This type of charge transfer (i.e., the initial sharp drop in the Mg_{cat} charge) failed to occur in the D256E enzyme (Fig. 8A).

Computational studies and the TS energy barrier in the D256E system

It is interesting to consider interactions that account for the higher TS energy barrier in the D256E system as compared with the wild-type system. The structures of the active sites of D256E and wild-type enzymes showed: (1) that a water molecule in D256E replaces OD2 of Asp256, but the glutamate carboxyl group's OE1 is near O3′. In the D256E and wild-type

systems, the alignment of O3′ with Pα and the bridging oxygen on the leaving group is similar. Thus, these features do not appear to account for the energy barrier difference; (2) Arg254 interacts with OD1 of Asp256 in the wild-type system, but does not interact with the glutamate side chain in the D256E system. This leads to a large impact on the energy decomposition in the two systems, in that Arg254 is stabilizing for the D256E system, but destabilizing for the wild-type system (Table 2). Based on this destabilizing effect in the wild-type system, one might expect the D256E system to have a lower energy barrier, instead of the higher barrier observed. Hence, the results of the energy decomposition for this single residue fail to offer a straightforward explanation of the experimental results (enzymatic rate for wild-type > D256E and QM/MM barrier D256E > wild-type). The destabilizing effect of Arg254 in the wild-type system may be due to charge repulsion during the proton jump to Asp256. Thus, the Arg254 destabilizing effect in the wild-type system (Table 2) can be rationalized; proton transfer from O3′ to Asp256 brings the proton closer to the positively charged guanidino group of Arg254, and the attendant repulsive effect is reflected in energy decomposition (Table 2). Yet, once the repulsion is overcome early in the reaction path, the reaction now experiences a lower energy barrier, as the appropriately charged O3′ and Pα interact.

Conclusion

Among the overarching features emerging from this work is the observation of the critical role of Arg254 in stabilizing the carboxylate of Asp256. From the results with the D256E mutant, proton transfer to the nearby, but unstabilized, glutamate carboxylate OE1 is insufficient to support O3′ proton transfer early in the reaction path, and to allow the mutant to mimic the wild-type enzyme's activity. Similarly, the D256E enzyme has a water molecule in proximity to O3′. Yet, the proximity of this water molecule was insufficient to allow it to accept the O3′ proton and substitute for OD2 of Asp256, as in the wild-type enzyme. These results point to the importance of a well-positioned stabilized carboxylate oxygen as acceptor of the O3′ proton, rather than an unstabilized carboxylate or nearby water molecule. Stabilization of the O3′ proton acceptor is probably not the only such stabilization effect in the quantum region of DNA polymerase active sites. The stabilization of the non-bridging oxygen on Pα of the incoming nucleotides may be an analogous situation. Consistent with this idea is the presence in several polymerases of an active site basic side-chain that interacts with the non-bridging oxygen on Pα, presumably stabilizing Pα during the bond-forming step of nucleotidyl transfer. Pol β does not have such a stabilizing side-chain for the non-bridging oxygen on Pα. It is intriguing that polymerases with this interaction are among the most efficient polymerases for correct nucleotide insertion and display high fidelity DNA synthesis.

Supplementary Material

Refer to Web version on PubMed Central for supplementary material.

Acknowledgments

This research was supported by Research Project Numbers Z01-ES050158 and Z01-ES050161 (SHW), Z01-ES043010 (LGP) and Z01-ES102645 (LCP) in the Intramural Research Program of the National Institutes of Health, National Institute of Environmental Health Sciences. LGP also acknowledges support from NIH HL-006350.

Bibliography

1. Yousefzadeh MJ, Wood RD. DNA Repair (Amst). 2013; 12:1. [PubMed: 23219161]
2. Hubscher U, Maga G, Spadari S. Annu Rev Biochem. 2002; 71:133. [PubMed: 12045093]

3. Lange SS, Takata K, Wood RD. Nat Rev Cancer. 2011; 11:96. [PubMed: 21258395]
4. Kunkel TA, Bebenek R. Annual Review of Biochemistry. 2000; 69:497.
5. Beese LS, Steitz TA. EMBO J. 1991; 10:25. [PubMed: 1989886]
6. Steitz TA, Steitz JA. Proceedings of the National Academy of Sciences of the United States of America. 1993; 90:6498. [PubMed: 8341661]
7. Deutscher MP, Kornberg A. J Biol Chem. 1969; 244:3019. [PubMed: 4306290]
8. Beard WA, Shock DD, Vande Berg BJ, Wilson SH. Journal of Biological Chemistry. 2002; 277:47393. [PubMed: 12370169]
9. Brody RS, Frey PA. Biochemistry. 1981; 20:1245. [PubMed: 7013792]
10. Cisneros GA, Perera L, Garcia-Diaz M, Bebenek K, Kunkel TA, Pedersen LG. DNA Repair. 2008; 7:1824. [PubMed: 18692600]
11. Liu HY, Zhang YK, Yang WT. Journal of the American Chemical Society. 2000; 122:6560.
12. Nakamura T, Zhao Y, Yamagata Y, Hua Y.-j. Yang W. Nature. 2012; 487:196. [PubMed: 22785315]
13. Lin P, Pedersen LC, Batra VK, Beard WA, Wilson SH, Pedersen LG. Proc. Natl. Acad. Sci. USA. 2006; 103:13294. [PubMed: 16938895]
14. Beard WA, Wilson SH. Methods Enzymol. 1995; 262:98. [PubMed: 8594388]
15. Batra VK, Beard WA, Shock DD, Krahn JM, Pedersen LC, Wilson SH. Structure (Camb). 2006; 14:757. [PubMed: 16615916]
16. Otwinowski Z, Minor W. Methods Enzymol. 1997; 276:307.
17. Pettersen EF, Goddard TD, Huang CC, Couch GS, Greenblatt DM, Meng EC, Ferrin TE. Journal of Computational Chemistry. 2004; 25:1605. [PubMed: 15264254]
18. Beard WA, Shock DD, Yang X-P, DeLauder SF, Wilson SH. J. Biol. Chem. 2002; 277:8235. [PubMed: 11756435]
19. Beard WA, Appleman JR, Delcamp TJ, Freisheim JH, Blakley RL. Journal of Biological Chemistry. 1989; 264:9391. [PubMed: 2498330]
20. Ellis KJ, Morrison JF. Methods in Enzymology. 1982; 87:405. [PubMed: 7176924]
21. Case, DA.; Darden, TA.; Cheatham, TE.; Simmerling, CL.; Wang, J.; Duke, RE.; Luo, R.; Crowley, M.; Walker, RC.; Zhang, W.; Merz, KM.; Wang, B.; Hayik, S.; Roitberg, A.; Seabra, G.; Kolossvary, I.; Wong, KF.; Paesani, F.; Vanicek, J.; Wu, X.; Brozell, SR.; Steinbrecher, T.; Gohlke, H.; Yang, L.; Tan, C.; Mongan, J.; Hornak, V.; Cui, G.; Mathews, DH.; Seetin, MG.; Sagui, C.; Babin, V.; Kollman, PA. Amber 11. University of California; 2010.
22. Hornak V, Abel R, Okur A, Strockbine B, Roitberg A, Simmerling C. Proteins. 2006; 65:712. [PubMed: 16981200]
23. Jorgensen WL, Chandrasekhar J, Madura JD, Impey RW, Klein ML. Journal of Chemical Physics. 1983; 79:926.
24. Darden T, York D, Pedersen L. Journal of Chemical Physics. 1993; 98:10089.
25. Essmann U, Perera L, Berkowitz ML, Darden T, Lee H, Pedersen LG. Journal of Chemical Physics. 1995; 103:8577.
26. Frisch, M.; Trucks, G.; Schlegel, H.; Scuseria, G.; Robb, M.; Cheeseman, J.; Zakrzewski, V.; Montgomery, J., Jr; Stratmann, R.; Burant, J. Gaussian Inc.; Wallingford, CT: 2009.
27. Dapprich S, Komaromi I, Byun KS, Morokuma K, Frisch MJ. Journal of Molecular Structure-Theochem. 1999; 461:1.
28. Lee CT, Yang WT, Parr RG. Physical Review B. 1988; 37:785.
29. Besler BH, Merz KM, Kollman PA. Journal of Computational Chemistry. 1990; 11:431.
30. Vande Berg BJ, Beard WA, Wilson SH. J. Biol. Chem. 2001; 276:3408. [PubMed: 11024043]
31. Sucato CA, Upton TG, Kashemirov BA, Osuna J, Oertell K, Beard WA, Wilson SH, Florian J, Warshel A, McKenna CE, Goodman MF. Biochemistry. 2008; 47:870. [PubMed: 18161950]
32. Balbo PB, Meinke G, Bohm A. Biochemistry. 2005; 44:7777. [PubMed: 15909992]
33. Adams PD, Afonine PV, Bunkoczi G, Chen VB, Davis IW, Echols N, Headd JJ, Hung L-W, Kapral GJ, Grosse-Kunstleve RW, McCoy AJ, Moriarty NW, Oeffner R, Read RJ, Richardson DC, Richardson JS, Terwilliger TC, Zwart PH. Acta Cryst. D. 2010; 66:213. [PubMed: 20124702]

34. Lin P, Batra VK, Pedersen LC, Beard WA, Wilson SH, Pedersen LG. Proc. Natl. Acad. Sci. USA. 2008; 105:5670. [PubMed: 18391201]

35. Jencks, WP.; Regenstein, J. CRC Handbook of Biochemistry. Sober, HA., editor. CRC Press; Boca Raton, FL: 1968. p. J150

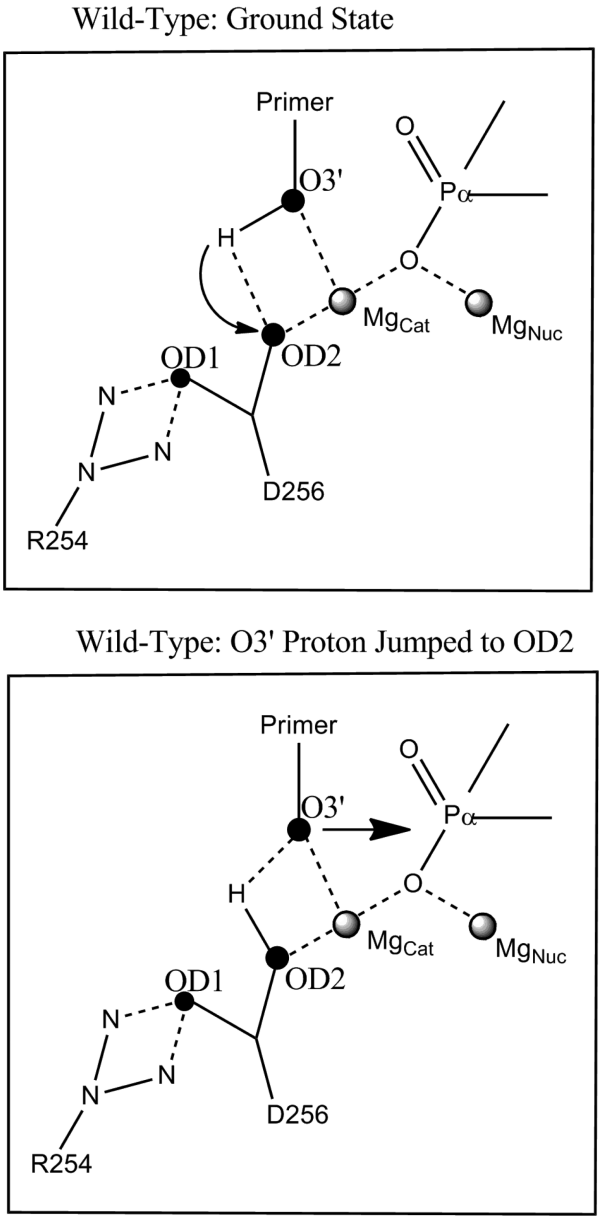

Scheme 1.
Proposed proton transfer from primer O3′ to Asp256 OD2.

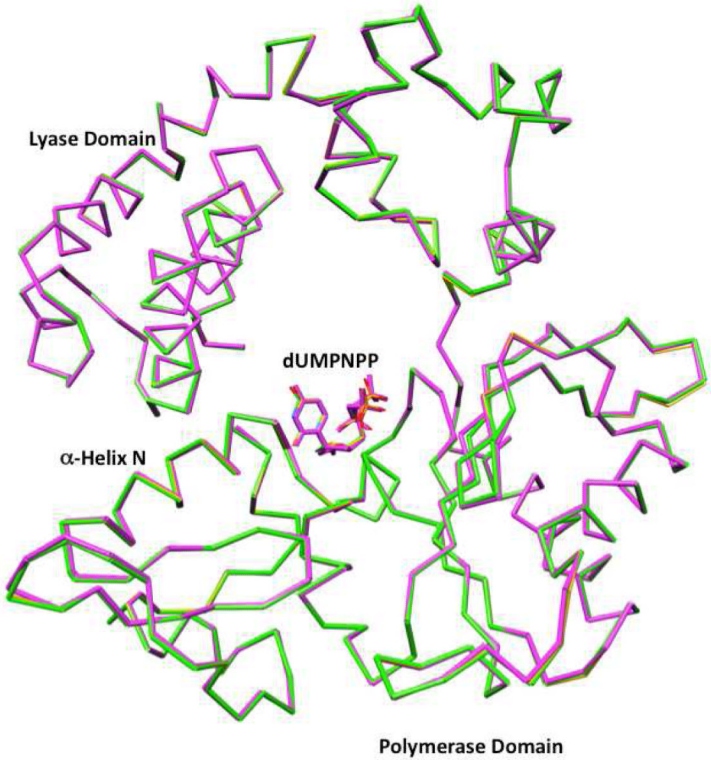

Figure 1. Illustration of the structures of closed conformations of the ternary substrate complexes of two mutant forms of pol β determined here and wild-type pol β

Representation of the wild-type pol β (PDB ID 2FMS, gold), D256E mutant (green) or D256A mutant (magenta) backbone (Cα) of the ternary substrate complexes with incoming nucleotide dUMPNPP opposite template A. The rmsd for all Cαs of D256E and D256A mutants relative to the wild-type enzyme are 0.17 and 0.22 Å, respectively. DNA is omitted for clarity, and dUMPNPP is shown (in the active site). The lyase and polymerase domains are labeled, as is α–Helix N that translocates upon closure.

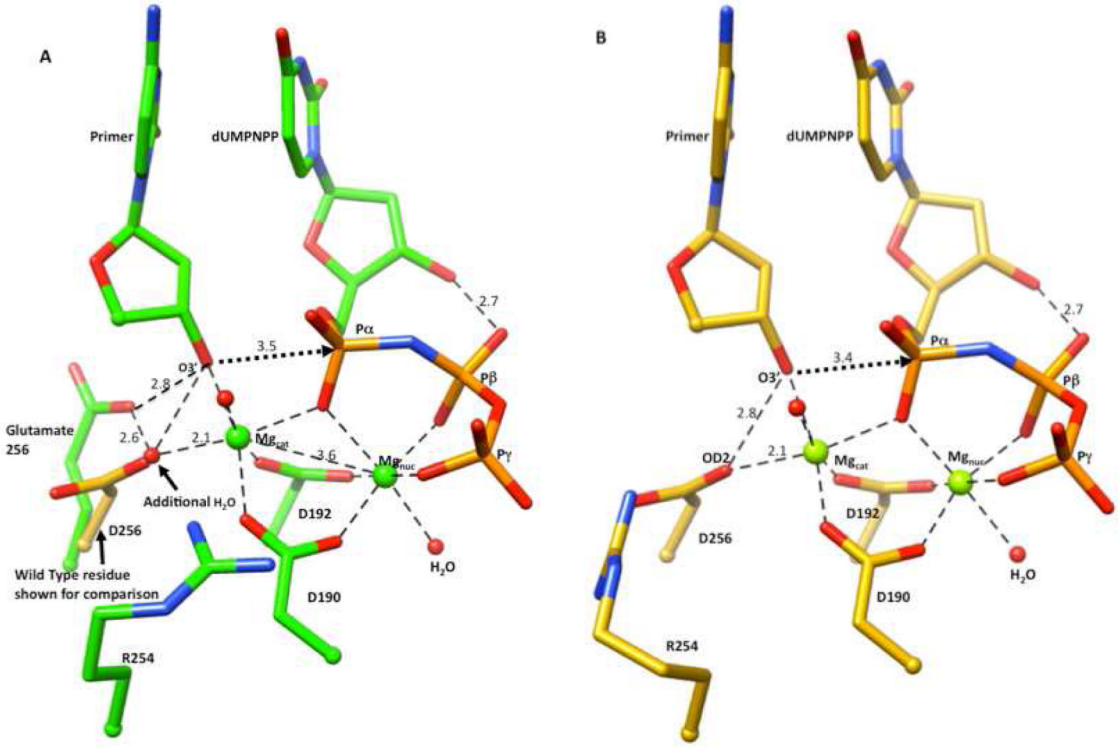

Figure 2. Active site geometry from the structure of the D256E mutant of pol β

(A) Illustration of the active site in the ternary substrate complex structure with incoming dUMPNPP. Relevant distances between the atoms are shown. The side chain of Glu 256 rotates, compared with D256 in wild-type, and does not interact directly with the catalytic metal. The space vacated by replacement of D256 OD2 is occupied by a water molecule ("additional water" and solid arrow). Although, the nucleotide binding metal (Mg_{nuc}) and catalytic metal (Mg_{cat}), shown in green, exhibit octahedral coordination similar to that in the wild-type enzyme, the catalytic metal utilizes the additional water molecule in place of OD2 of D256; the position of the side chain of wild-type D256 is shown in gold for comparison. The distance between O3′ and Pα (3.5 Å; dashed arrow) is similar to that in the wild-type enzyme. The position of the R254 side chain also is shown. (B) Illustration of the active site geometry of wild-type pol β, shown for comparison with panel A. The labeling is similar to that in panel A; the nucleotides and side chains are in gold.

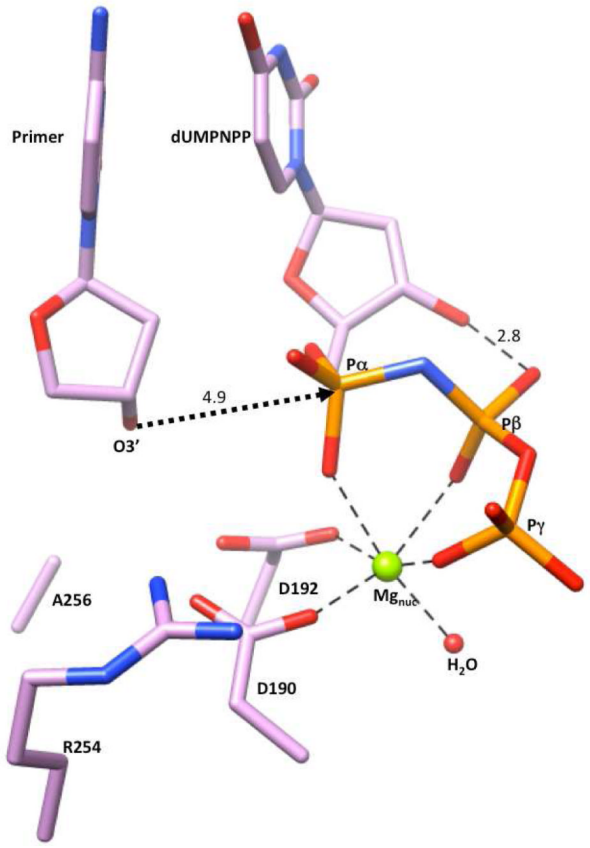

Figure 3. Active site geometry from the structure of the D256A mutant of pol β

The ternary substrate complex structure with an incoming dUMPNPP shows that in absence of the D256 side chain, there is no occupancy of the Mg_{cat} site. Mg_{nuc} exhibits octahedral coordination similar to that in the wild-type enzyme. The sugar pucker of the primer terminus is in 2'-endo conformation leading to an increased distance (4.9 Å vs. 3.4 Å in the wild-type enzyme) between O3′ of the primer terminus and Pα of the incoming nucleotide. R254 is rotated away from its position in wild-type into a position similar to that seen in D256E structure. The nucleotides and side chains are shown in magenta.

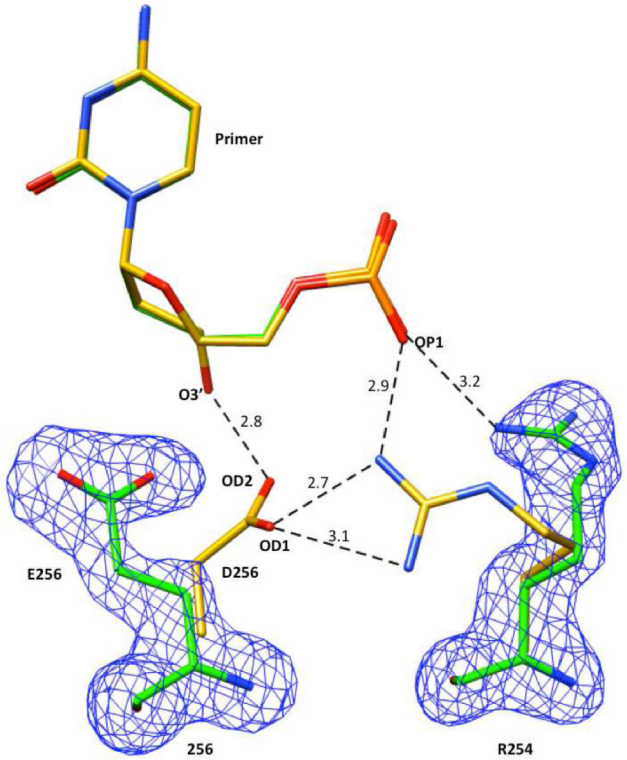

Figure 4. Disruption of the R254:D256 salt-bridge observed in the structure of the D256E mutant enzyme

Superposition of structures of the wild-type (gold) and D256E (green) enzymes. The primer nucleotide is shown. In the wild-type enzyme (gold), the guanidino group of Arg254 stabilizes D256 by a salt-bridge interaction to its OD1. This interaction is lost in the mutant enzyme due to the novel positions of both the R254 and E256 (green). The primer terminus sugar pucker conformation (3'-endo) is the same in both structures. The simulated annealing fo-fc electron density omit maps (blue) for R254 and D256E, contoured at 5σ, are shown.

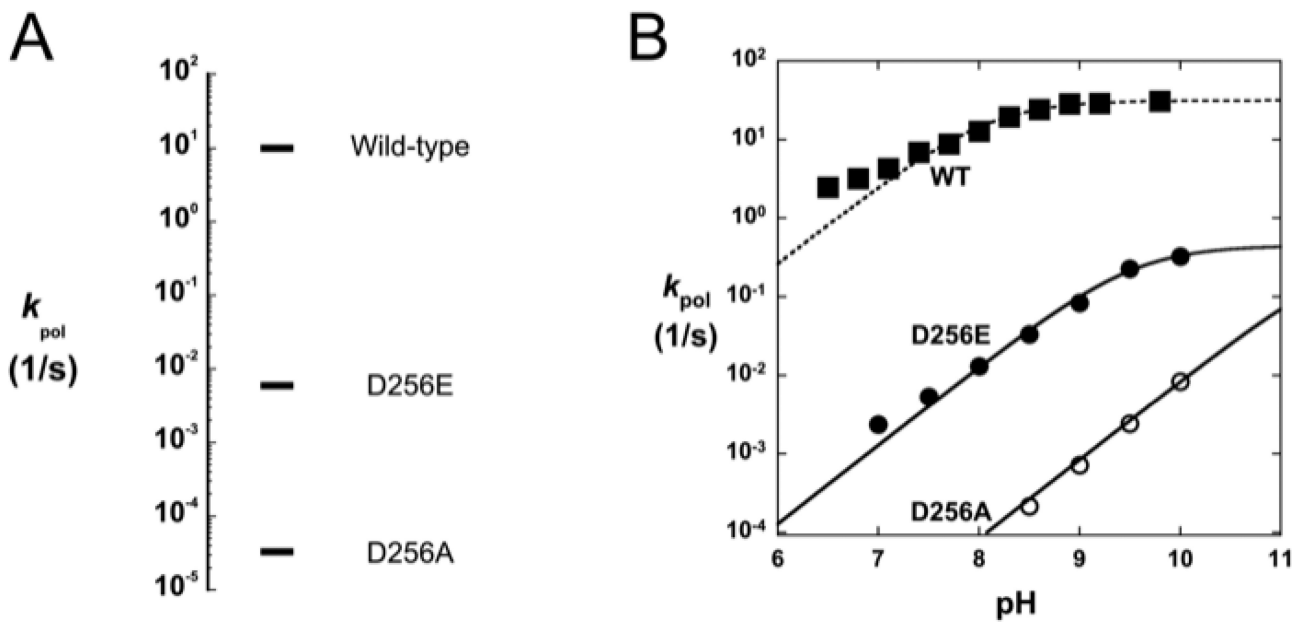

Figure 5. The pH-dependence of the insertion rate on the identity of residue 256 of pol β

The insertion rate (k_{pol}) was measured by single-turnover analysis on single-nucleotide gapped DNA substrates as described under Experimental Design. (A) The insertion rate for wild-type enzyme was taken from Vande Berg et al. (2001).[30] The activities were determined at pH 7.4 (37 °C). The value for the D256A mutant is based on a single time-point (>1 h) due to the extremely low activity of this mutant. However, it is in-line with the value that can be extrapolated from its pH profile. (B) The pH dependence of dCTP insertion. Wild-type data is from Sucato et al.[31] The solid lines show fits of the data to a function for a single-ionization yielding pK_as of 8.1 ± 0.05 (wild-type, WT), 9.5 ± 0.07 (D256E) and 11.7 ± 2.3 (D256A).

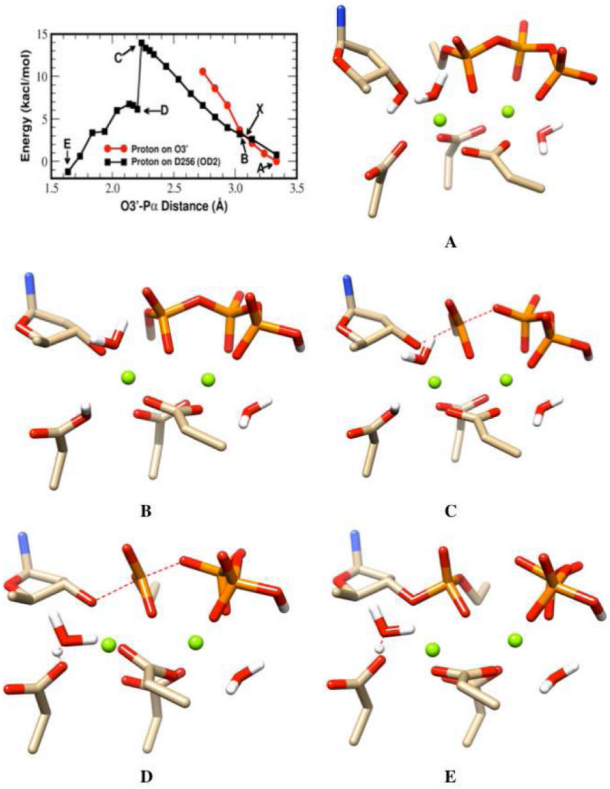

Figure 6. Energy profile of the reaction path and QM region structures for the wild-type enzyme at points along the reaction path as the distance between O3′ and Pα decreases

The energies represented by closed red circles correspond to configurations in which the proton is attached to O3′. The energies represented by closed black squares correspond to configurations in which the proton originally attached to O3′ is transferred onto OD2 of D256, at point X in the diagram. In the diagram, A, B, C, D and E represent different points along the reaction path, from the ground state (A) to the product state (E). Point C is the transition state. The structures shown correspond to the points indicated along the reaction path. At points D and E the water molecule attached to the catalytic magnesium has transferred to OD2 of D256. The transition state structure is illustrated in C.

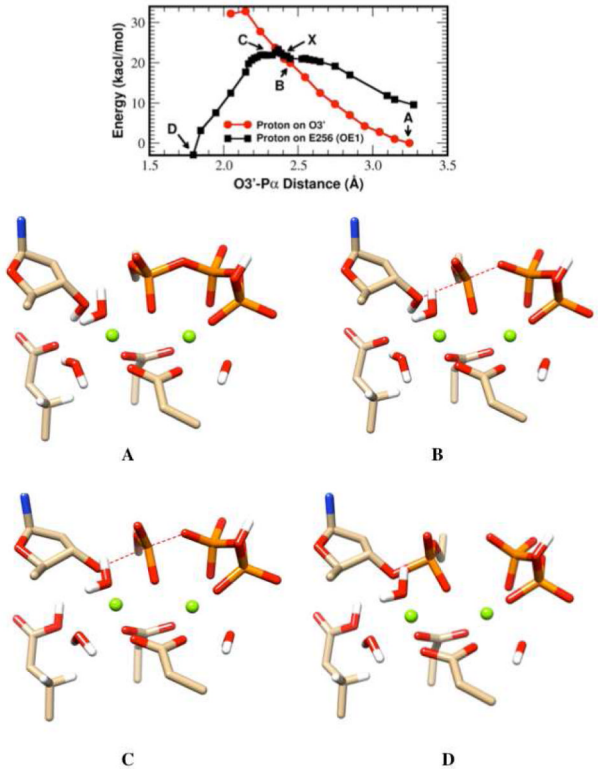

Figure 7. Energy profile of the reaction path and QM region structures for the D256E enzyme at points along the reaction path as the distance between O3′ and Pα decreases

The energies represented by closed black squares correspond to configurations in which the proton is attached to OE1, whereas those represented by closed red circles correspond to configurations in which the proton is attached to O3′. In the diagram, A, B, C, and D represent different points along the reaction path, from the ground state (A) to the product state (D). Point C is the transition state (TS). The structures shown correspond to the points indicated along the reaction path. The proton is transferred onto OE1 of E256 at point X in the diagram; the structure at point B shows that the proton is still attached to O3′. Two water molecules are shown coordinating with the catalytic magnesium. The transition state structure is illustrated in C.

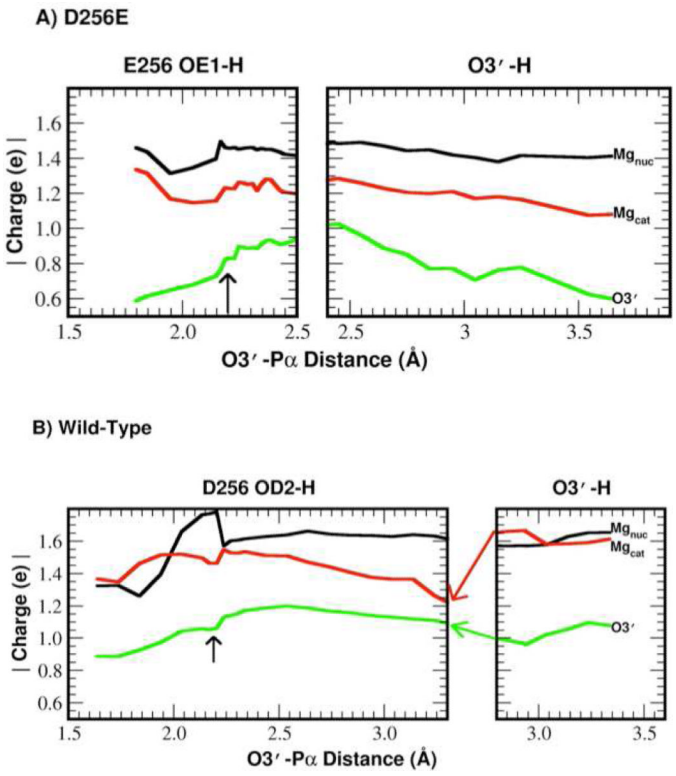

Figure 8. Charges on O3′ and the divalent metal ions calculated by the MK method (Y1[29]) for the wild-type and D256E configurations selected in the QM energy calculations of Figures 5 and 6

A) For the D256E enzyme (E256), in the right panel charges are calculated when the proton is attached to O3′. The panel on the left shows charges on the corresponding atoms, when the proton that was initially bound to O3′ has transferred onto E256. The nucleotide-binding magnesium – black; catalytic magnesium – red; O3′ of the primer terminal – green. The position of the proton is shown at the top, and the O3′ to Pα distance and charge are shown. The small arrow in the left panel indicates the TS. Note that the absolute values of the charge are shown. B) For the wild-type enzyme, in the right panel, charges are calculated when the proton is attached to O3′. The panel on the left shows charges on the corresponding atoms, when the proton initially bound to O3′ is transferred onto D256. The color designations are the same as in panel A. The red and green arrows between the panels illustrate the charge differences upon proton transfer for the Mg_{cat} and O3′ atoms, respectively. The small arrow in the left panel indicates the TS.

Table 1

Crystallographic Statistics

	DNA Polymerase β Mutant	
	D256E	**D256A**
Data Collection		
Space Group	$P2_1$	$P2_1$
a (Å)	50.66	50.43
b (Å)	79.76	79.81
c (Å)	55.64	55.34
β (°)	107.47	107.23
d_{min} (Å)	2.00	2.39
R_{merge} (%)[a]	0.089 (0.446)	0.089 (0.440)
Completeness (%)	99.1 (96.8)	99.0 (91.3)
Unique Reflections	28347 (2747)	16387 (1509)
Total Reflections	100123	54888
I/σ	11.8 (2.76)	10.3 (2.07)
Refinement		
r.m.s. deviations		
Bond lengths (Å)	0.005	0.008
Bond angles (°)	1.047	1.532
R_{work} (%)	19.20	17.75
R_{free} (%)	23.26	25.78
Average B Factors (Å)		
Protein	23.93	30.12
DNA	32.94	31.12
Ramachandaran Analysis (%)		
Favored	98.5	96.9
Allowed	100	100
RSCB ID	4JWM	4JWN

[a]Numbers in the parentheses refer to the data in the highest resolution shell

Table 2

The electrostatic effects of non-quantum region residues on the transition states for the D256E and wild-type systems.

Residue	D256E	Wild-type
Arg 40	−4.89	−4.83
Arg 149	−6.85	−3.99
Ser 180	−4.51	−1.23
Arg 183	−14.74	−20.96
Lys 234	10.39	3.59
Arg 254	−5.98	33.37
Arg 258	8.83	0.91
Asp 276	6.16	10.15
Glu 295	−3.32	0.88
Glu 335	7.58	10.26